Ferroelectric Materials

Deutsche Ausgabe: DOI: 10.1002/ange.201805071
Internationale Ausgabe: DOI: 10.1002/anie.201805071

Room-Temperature Ferroelectricity in an Organic Cocrystal

*Ren A. Wiscons[+], N. Rajesh Goud[+], Joshua T. Damron, and Adam J. Matzger**

Abstract: *Ferroelectric materials exhibit switchable remanent polarization due to reversible symmetry breaking under an applied electric field. Previous research has leveraged temperature-induced neutral-ionic transitions in charge-transfer (CT) cocrystals to access ferroelectrics that operate through displacement of molecules under an applied field. However, displacive ferroelectric behavior is rare in organic CT cocrystals and achieving a Curie temperature (T_C) above ambient has been elusive. Here a cocrystal between acenaphthene and 2,3,5,6-tetrafluoro-7,7,8,8-tetracyanoquinodimethane is presented that shows switchable remanent polarization at room temperature ($T_C = 68\,°C$). Raman spectroscopy, X-ray diffraction, and solid-state NMR spectroscopy indicate the ferroelectric behavior is facilitated by acenaphthene (AN) rotation, deviating from conventional design strategies for CT ferroelectrics. These findings highlight the relevance of non-CT interactions in the design of displacive ferroelectric cocrystals.*

Crystalline charge-transfer (CT) complexes formed between neutral molecular components demonstrate a broad range of fractional electron transfer that predicates applications in most fields of electronics.[1] With benefits offered by solution processability, flexibility, reduced toxicity, and ease of tunability, synthesis, and purification, organic electronic materials are promising alternatives to traditional inorganics.[1g,2] Of particular interest is the application of CT cocrystals as displacive ferroelectrics in data storage.[2c,3] The exchangeable nature of the CT pair permits rapid screening of various molecular combinations relative to single-component materials; this is advantageous in the field of ferroelectric materials, which show stringent and statistically disfavored crystallographic requirements. Taking advantage of this design feature, several organic CT ferroelectrics have been reported,[1d,e,2,4] although most of materials that have been discovered to date only exhibit ferroelectricity below room temperature.

Conventional design strategies towards displacive ferroelectric cocrystals focus on tailoring the CT gap in 1D chains of alternating π-electron donor (D) and acceptor (A) molecules to achieve a transition between neutral ($DADA\ldots$) and ionic ($D^+A^-\ D^+A^-\ldots$) solid phases (NI transition)[5] through a reversible Peierls-type lattice instability at the Curie temperature, T_C.[1b–e,i,2–4,6] The Peierls distortion can manifest as a molecular deformation (Figure 1a) or displacement (Figure 1b) that polarizes the CT chain in the ionic/ferroelectric phase.[1e,3] However, design strategies that leverage electronic instabilities modeled in 1D CT chains are limited in their ability to predict interchain interactions that may prevent structural transitions. We argue that the paucity of reported cocrystals that exhibit room-temperature displacive ferroelectricity is due, in part, to design strategies that consider CT interactions as the driving force for the paraelectric–ferroelectric transition, while assuming that interchain interactions are non-participatory.

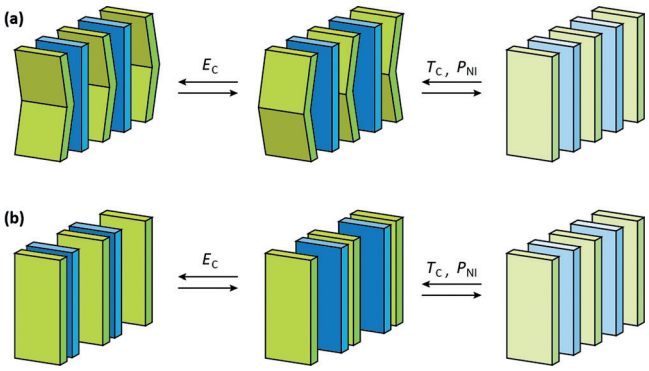

Figure 1. Two mechanisms of displacive ferroelectric transitioning in CT cocrystals: a) molecular deformation and b) molecular displacement (adapted from Horiuchi et al.).[1e] The polarization direction can be switched under a coercive electric field, E_C, and the ferroelectric–paraelectric transition can be thermally induced at the T_C or the NI transition pressure, P_{NI}.

Herein, a room-temperature displacive ferroelectric CT cocrystal formed between acenaphthene (AN) and 2,3,5,6-tetrafluoro-7,7,8,8-tetracyanoquinodimethane (F_4TCNQ) is presented. A record high T_C of 68 °C allows room-temperature ferroelectricity in AN-F_4TCNQ; the T_C corresponds to an activated by rotational motion in AN that decouples AN-F_4TCNQ dimers, evenly spacing D and A molecules within the CT π-stacks. Weak electronic coupling between AN and F_4TCNQ, as measured by Raman spectroscopy, supports the claim that the mechanism of the ferroelectric–paraelectric transition is primarily structural. No formal NI transition occurs at the T_C although this material displays switchable remanent polarization, prompting re-evaluation of conventional redox potential-focused design strategies. AN-F_4TCNQ highlights the importance of interchain interactions and molecular dynamics in the design of CT cocrystals that undergo ferroelectric transitions and provides critical insights

[*] R. A. Wiscons,[+] Dr. N. R. Goud,[+] Dr. J. T. Damron, Prof. A. J. Matzger
Department of Chemistry and the Macromolecular Science and Engineering Program, University of Michigan
930 North University Avenue, Ann Arbor, MI 48109-1055 (USA)
E-mail: matzger@umich.edu
[+] These authors contributed equally to this work.
Supporting information and the ORCID identification number(s) for the author(s) of this article can be found under: https://doi.org/10.1002/anie.201805071.

to improve the diversity and reliability of subsequent ferroelectric design strategies.

AN and F_4TCNQ (Figure 2a) were selected as cocrystallization partners because they display a minimal calculated

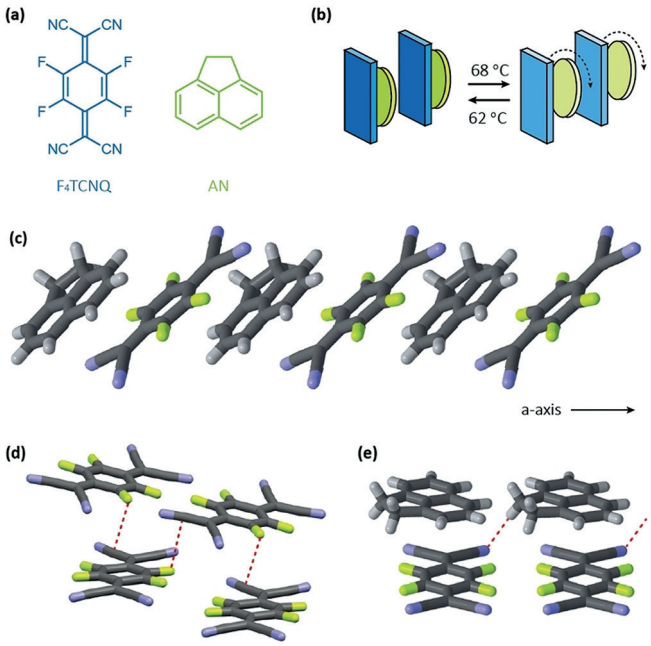

Figure 2. a) Chemical structures of F_4TCNQ (blue) and AN (green); b) illustration summarizing the NI transition between the low-temperature *Pc* (left) and high-temperature $P2_1/c$ (right) phases with the dashed arrow representing the high-temperature rotational disorder; c) 1D chains of alternating AN and F_4TCNQ molecules along the *a*-axis from the room-temperature crystal structure; d) chains of C–F···C≡N interactions formed between neighboring F_4TCNQ molecules; e) view highlighting the C≡N···H–C interactions.[14]

difference in position of the HOMO and LUMO energy levels for isolated gas-phase *D* and *A* molecules. This approach is consistent with current strategies towards CT cocrystal design.[1f,h] Cocrystals of AN-F_4TCNQ were grown by solvent evaporation from an equimolar acetonitrile solution (see Supporting Information). Thermal cycling by differential scanning calorimetry (DSC) revealed a reversible endotherm upon heating at 341.1 K (68.1 °C) and an exotherm at 335.0 K (62.0 °C) upon cooling. Single-crystal XRD (SCXRD) structures were obtained at 85 K, 293 K (20 °C), and 348 K (75 °C). At both 85 K and 293 K, the cocrystal solves in the polar *Pc* space group, whereas the 348 K crystal structure becomes centrosymmetric ($P2_1/c$). AN-F_4TCNQ adopts a mixed-stack motif parallel to the *a*-axis (Figure 2c). Interplanar spacings reveal that the molecules are dimerized (D^+A^- D^+A^-…) in the two low-temperature structures with alternating long and short π-stacking distances (3.415 Å and 3.369 Å at 293 K measured *D* centroid to *A* plane), while the high-temperature crystal structure is differentiated by a decoupling of the *DA* dimers, evenly spacing the *D* and *A* molecules (3.461 Å), and a 180° rotational disorder of AN. Despite this rotational disorder, 3D crystallinity is maintained in the $P2_1/c$ phase with close interchain contacts formed between C–F and C≡N on neighboring F_4TCNQ molecules (Figure 2d). These contacts are present in the *Pc* (at 293 K) and $P2_1/c$ phases at distances between 3.05 and 3.07 Å. Furthermore, the interchain contacts are strengthened through C≡N···H–C interactions[7] that are present in all three crystal structures at an interaction distance of 2.46 Å at 293 K (normalized hydrogen positions, Figure 2e).

Given that the phase change in AN-F_4TCNQ is accompanied by a reversible symmetry change (noncentrosymmetric to centrosymmetric), the room-temperature ferroelectricity was investigated by measuring polarization hysteresis parallel to the CT stacking direction (*a*-axis) on single crystals (see Supporting Information). Polarization hysteresis loops measured directly show dielectric leakage that becomes more dramatic upon scanning to lower frequencies. Positive-up-negative-down (PUND) pulse measurements reveal that two components (dielectric and ferroelectric) contribute to the overall polarization intensity and, at a frequency optimized for the ferroelectric component, the dielectric component contributes to 95% of the overall intensity and the ferroelectric component the other 5% (see Supporting Information). The dielectric component is likely associated with rotation of AN under an applied electric field due to its dipole moment, which is consistent with the increased motion of AN observed in the crystal structure of the high-temperature $P2_1/c$ phase. Remanent polarization hysteresis loops were measured using a double triangular waveform voltage to remove the effects of non-hysteresis character (see Supporting Information). Room-temperature ferroelectricity in AN-F_4TCNQ was confirmed and the remanent polarization (*Pr*) was measured up to 0.08 ± 0.01 nC cm^{-2} (see Supporting Information). By comparison to the model displacive ferroelectric formed between tetrathiafulvalene (TTF) and *p*-chloranil (CA), the *Pr* of AN-F_4TCNQ is small; however, AN-F_4TCNQ represents remarkable progress for displacive ferroelectric cocrystals as it displays ferroelectric behavior above room temperature, while TTF-CA is only ferroelectric below 81 K. Electronic coupling between AN and F_4TCNQ was further characterized by calculating the ionicity (ρ) of the cocrystal during the ferroelectric–paraelectric transition. Ionicity values were calculated from Raman spectra[1h,8] obtained between 30 and 80 °C, revealing a minor shift in ionicity between 65 and 70 °C associated with the transition (see Supporting Information). The ρ of the ionic phase was calculated at 0.3 e, which decreases to 0.2 e upon transitioning to the $P2_1/c$ phase. The $\Delta\rho$ for this material is 0.1 e (about one fourth that of TTF-CA), implicating that a *true* NI transition[8b] is not crossed.

By assuming a double-well potential model for a ferroelectric transition,[9] the T_C can be used to estimate the energy difference between the ferroelectric and paraelectric states. Participation of non-CT interactions altered during the transition can be probed by comparing the T_C of non-deuterated and perdeuterated analogues of ferroelectric materials. For example, TTF-CA exhibits a T_C 2–5 K lower than d_4TTF-CA,[1e,10] which was attributed to lengthening, destabilization, and symmetrization of interchain C–H···O hydrogen bonds upon transitioning to the paraelectric (neutral) phase.[11]

Investigation into the ferroelectric–paraelectric transition mechanism for AN-F_4TCNQ began with synthesis of d_{10}AN-F_4TCNQ. The DSC trace revealed a reversible endotherm at 69.2 °C upon heating and an exotherm at 62.0 °C upon cooling. The 1.1 °C increase in T_C upon deuteration is in the opposite direction of what would be expected for a change in redox potential due to the reduced hyperconjugative stabilization afforded by deuterium. This observation indicates that non-CT interactions contribute to the ferroelectric–paraelectric transition mechanism (vide infra).

Examples of flip-flop[12a] and plastic[12b] ferroelectricity in CT metal–organic systems and antiferroelectric–paraelectric transitions in organic crystals[12c] have suggested the possibility of forming ferroelectrics in which structural transitions are controlled by activated vibrational and/or rotational modes. Such a mechanism would be consistent with the AN motion identified by SCXRD and dielectric leakage observed during polarization measurements. Evidence of dynamic molecular rotation was collected by solid-state ^{1}H magic-angle-spinning nuclear magnetic resonance (MAS-NMR) spectroscopy between 30 and 80 °C. Above 60 °C, the aromatic and non-aromatic proton environments in AN can be differentiated in the 1D ^{1}H spectra (Figure 3a); however, with a decrease in temperature, the methylene signal shifts downfield, appearing as a shoulder on the aromatic peak, while the aromatic signal shows progressive broadening upon cooling. The sharpening upon heating from 30 to 60 °C suggests that the transition is preceded by continuous structural changes and confirms that the AN rotational disorder observed by SCXRD is dynamic. The ^{1}H T_1 relaxation data collected between 30 and 80 °C is most suitably fit with a bicomponent T_1 curve (see Supporting Information). Both components show a decrease in relaxation time upon heating to 60 °C, which is likely a product of two effects: a decrease in CT and interruption of C≡N···H–C interactions due to rotational motion. At temperatures beyond 60 °C, an increase in the T_1 is measured, caused by a freeing of AN motion, pushing the dynamics past the T_1 minimum and lengthening the T_1 time. At and above the T_C, this effect becomes more dramatic (Figure 3b).

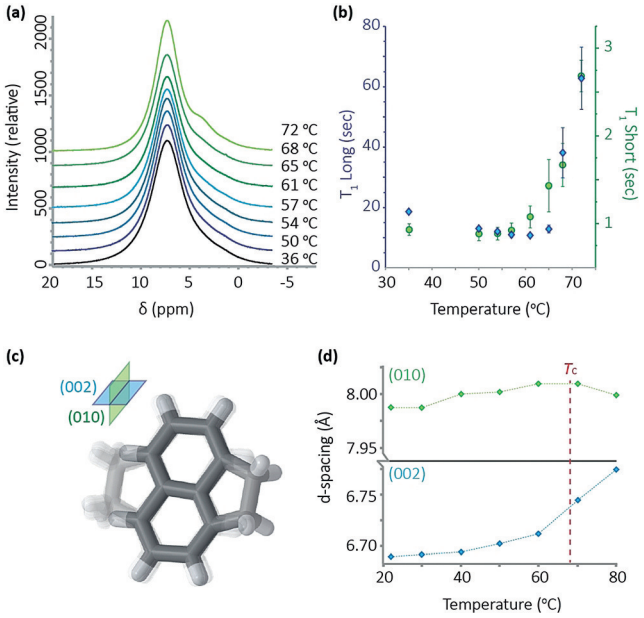

Figure 3. a) 1D MAS-NMR ^{1}H spectra collected between 30 and 80 °C; b) T_1 relaxation time for the long (blue) and short (green) components as a function of temperature; c) orientation of AN relative to the (002) and (010) Miller planes; d) *d*-spacing expansion between the (010) and (002) Miller planes with increasing temperature.

The MAS-NMR studies prompted a targeted investigation of the C≡N···H–C interaction during the ferroelectric–paraelectric transition. Classical C≡N···H–O H-bonds show $-\Delta H°$ between 2–5 kcal mol^{-1}[13] (likely lower in AN-F_4TCNQ due to the weaker donation), too low of an energetic barrier to independently prevent AN rotational motion at room temperature. The barrier to rotation is likely a convolution of the C≡N···H–C interaction and lattice reorganization enthalpies to accommodate AN rotation. The relative significances of these effects to the structural phase transition were studied by powder-XRD (PXRD) and confirmed by SCXRD (see Supporting Information). The 2θ shift in the reflections associated with the (010) and (002) interplanar spacings were monitored between 20 and 80 °C as these planes describe crystallographic expansions/contractions due to C≡N···H–C interactions and rotation-induced lattice deformation, respectively (Figure 3c). As shown in Figure 3d, the reflection corresponding to the (010) plane does not significantly shift during the transition, indicating that destabilization and elongation of the C≡N···H–C interaction is not a dominant contributor to the structural transition observed by XRD. Contrastingly, the {002} interplanar spacings dramatically expand ≈5 °C before the T_C. Activation of AN rotation is consistent with the preferential interplanar expansion between the (002) planes, which would account for additional enthalpic contributions to the barrier preventing ferroelectric–paraelectric transitioning at room temperature.

It has been shown that AN-F_4TCNQ undergoes a space group change from *Pc* to $P2_1/c$ at 68 °C associated with a decrease in ionicity, consistent with a ferroelectric–paraelectric phase transition, despite weak electronic coupling between AN and F_4TCNQ. Activation of AN rotational motion was found to accompany the phase transition as shown by MAS-NMR and PXRD. Reversible remanent polarization of AN-F_4TCNQ was measured, confirming that this material is ferroelectric at room temperature although the mechanism of transition is primarily structural. Given these findings, we suggest inclusion of interchain interactions and molecular dynamics that facilitate displacement events responsible for polarization switching in future design of ferroelectric CT cocrystals. Shifting from electronically-driven to structure-driven mechanisms allows a greater diversity of materials that undergo lattice-facilitated ferroelectric–paraelectric transitions to be accessed that may not be predicted by a 1D Peierls distortion model.

Acknowledgements

This work was supported by the Army Research Office (ARO) in the form of a Multidisciplinary University Research Initiative (MURI) (grant number: W911NF-13-1-

0387). The authors would also like to acknowledge J. Kampf for single-crystal X-ray structures of AN-F_4TCNQ, G. J. Rosenhauer for contributing to experimental design, and Professor John Heron for assistance with collecting polarization hysteresis loops.

Conflict of interest

The authors declare no conflict of interest.

Keywords: charge transfer · crystal engineering · ferroelectrics · organic electronics · polarization

How to cite: *Angew. Chem. Int. Ed.* **2018**, *57*, 9044–9047
Angew. Chem. **2018**, *130*, 9182–9185

[1] a) Z. G. Soos, *Annu. Rev. Phys. Chem.* **1974**, *25*, 121–153; b) J. B. Torrance, J. E. Vazquez, J. J. Mayerle, V. Y. Lee, *Phys. Rev. Lett.* **1981**, *46*, 253–257; c) J. B. Torrance, A. Girlando, J. J. Mayerle, J. I. Crowley, V. Y. Lee, P. Batail, *Phys. Rev. Lett.* **1981**, *47*, 1747–1750; d) S. Horiuchi, Y. Okimoto, R. Kuami, Y. Tokura, *J. Am. Chem. Soc.* **2001**, *123*, 665–670; e) S. Horiuchi, R. Kumai, Y. Okimoto, Y. Tokura, *Chem. Phys.* **2006**, *325*, 78–91; f) I. Shokaryev, A. J. C. Buurma, O. D. Jurchescu, M. A. Uijttewaal, G. A. de Wijs, T. T. M. Palstra, R. A. de Groot, *J. Phys. Chem. A* **2008**, *112*, 2497–2502; g) K. P. Goetz, D. Vermeulen, M. E. Payne, C. Kloc, L. E. McNeil, O. D. Jurchescu, *J. Mater. Chem. C* **2014**, *2*, 3065–3076; h) N. R. Goud, A. J. Matzger, *Cryst. Growth Des.* **2017**, *17*, 328–336; i) S. Horiuchi, Y. Okimoto, R. Kumai, Y. Tokura, *Science* **2003**, *299*, 229–232.

[2] a) A. S. Tayi, A. Kaeser, M. Matsumo, T. Aida, S. I. Stupp, *Nat. Chem.* **2015**, *7*, 281–292; b) S. Horiuchi, F. Ishii, R. Kumai, Y. Okimoto, H. Tachibana, N. Nagaosa, Y. Tokura, *Nat. Mater.* **2005**, *4*, 163–166; c) S. Chen, C. Z. Xiao, *J. Am. Chem. Soc.* **2014**, *136*, 6428–6436.

[3] S. Horiuchi, Y. Tokura, *Nature* **2008**, *7*, 357–366.

[4] A. S. Tayi, A. K. Shveyd, A. C.-H. Sue, J. M. Szarko, B. S. Rolczynski, D. Cao, T. J. Kennedy, A. A. Sarjeant, C. L. Stern, W. F. Paxton, W. Wu, S. K. Dey, A. C. Fahrenbach, J. R. Guest, H. Mohseni, L. X. Chen, K. L. Wang, J. F. Stoddart, S. I. Stupp, *Nature* **2012**, *488*, 485–489.

[5] a) H. M. McConnell, B. M. Hoffman, R. M. Metzger, *Proc. Natl. Acad. Sci. USA* **1965**, *53*, 46–50; b) C. K. Prout, J. D. Wright, *Angew. Chem. Int. Ed. Engl.* **1968**, *7*, 659–667; *Angew. Chem.* **1968**, *80*, 688–697.

[6] a) S. Horiuchi, K. Kobayashi, R. Kuami, N. Minami, F. Kagawa, Y. Tokura, *Nat. Commun.* **2015**, *6*, 1–7; b) J. Hubbard, J. B. Torrance, *Phys. Rev. Lett.* **1981**, *47*, 1750–1754; c) F. Kagawa, S. Horiuchi, M. Tokunaga, J. Fujioka, Y. Tokura, *Nat. Phys.* **2010**, *6*, 169–172.

[7] R. Taylor, O. Kennard, *J. Am. Chem. Soc.* **1982**, *104*, 5063–5070.

[8] a) A. Salmerón-Valverde, J. G. Robles-Martínez, J. García-Serrano, R. Gómez, R. M. Ridaura, M. Quintana, A. Zehe, *Mol. Eng.* **1999**, *8*, 419–426; b) N. Castagnetti, G. Kociok-Köhn, E. Da Como, A. Girlando, *Phys. Rev. B* **2017**, *95*, 1–7; c) M. Masino, A. Girlando, A. Brillante, *Phys. Rev. B* **2007**, *76*, 1–7; d) A. Dengl, R. Beyer, T. Peterseim, T. Ivek, G. Untereiner, M. Dressel, *J. Chem. Phys.* **2014**, *240*, 1–6.

[9] N. Hill, *J. Phys. Chem. B* **2000**, *104*, 6694–6709.

[10] S. Horiuchi, R. Kumai, Y. Okimoto, Y. Tokura, *Synth. Met.* **2003**, *133–134*, 615–618.

[11] P. Batail, S. J. LaPlaca, J. J. Mayerle, J. B. Torrance, *J. Am. Chem. Soc.* **1981**, *103*, 951–953.

[12] a) T. Akutagawa, H. Koshinaka, D. Sato, S. Takeda, S.-I. Noro, H. Takakashi, R. Kumai, Y. Tokura, T. Nakamura, *Nat. Mater.* **2009**, *8*, 342–347; b) J. Harada, T. Shimojo, H. Oyamaguchi, H. Hasegawa, Y. Takahashi, K. Satomi, Y. Sazuki, J. Kawamata, T. Inabe, *Nat. Chem.* **2016**, *8*, 946–952; c) J.-I. Ichikawa, N. Hoshino, T. Takeda, T. Akutagawa, *J. Am. Chem. Soc.* **2015**, *137*, 13155–13160.

[13] a) J.-Y. Le Questel, M. Berthelot, C. Laurence, *J. Phys. Org. Chem.* **2000**, *13*, 347–358; b) M. Domagała, S. J. Grabowski, *J. Phys. Chem. A* **2005**, *109*, 5683–5688.

[14] CCDC 1840748–1840751 contain the supplementary crystallographic data for this paper. These data can be obtained free of charge from The Cambridge Crystallographic Data Centre.

Manuscript received: May 1, 2018
Accepted manuscript online: May 22, 2018
Version of record online: June 14, 2018

